NTIA Technical Memorandum TM-05-426

Radiation Pattern Analysis of a Four-Element Linear Array

John J. Lemmon

technical memorandum

U.S. DEPARTMENT OF COMMERCE · National Telecommunications and Information Administration

NTIA Technical Memorandum TM-05-426

Radiation Pattern Analysis of a Four-Element Linear Array

John J. Lemmon

U.S. DEPARTMENT OF COMMERCE
Carlos M. Gutierrez, Secretary

Michael D. Gallagher, Assistant Secretary
for Communications and Information

July 2005

DISCLAIMER

Certain commercial equipment, software, or materials are identified in this report to specify the technical aspects of the reported results. In no case does such identification imply recommendation or endorsement by the National Telecommunications and Information Administration, nor does it imply that the material or equipment identified is necessarily the best available for the purpose.

CONTENTS

RADIATION PATTERN ANALYSIS OF A FOUR-ELEMENT LINEAR ARRAY

John J. Lemmon[1]

The effects of mutual coupling on the radiation pattern of a four-element linear array were investigated. The objective was to improve the angular resolution of the array for direction-of-arrival estimation by compensating for mutual coupling. It is concluded that the effects of mutual coupling on the performance of the array are not significant, and that the angular resolution of the array is consistent with its theoretical radiation pattern in the absence of mutual coupling. However, it is recommended that the array be calibrated to compensate for systematic errors and any (small) mutual coupling effects that are present.

Key words: direction-of-arrival (DOA); linear array; mutual coupling

1. INTRODUCTION AND BACKGROUND

Several years ago Wilson and Papazian described direction-of-arrival (DOA) measurements using a four-element linear array [1]. Although the results demonstrate that their measurement system is indeed capable of determining the DOA of received signals, the authors expected the system to have better angular resolution than that inferred from angular power spectra developed from the measured data.[2] They further speculated that the relatively poor angular resolution was due to mutual coupling among the antenna elements.[2]

The purpose of the present study was to investigate the effects of mutual coupling on the radiation pattern of the antenna array used for these measurements and to determine how these effects could be taken into account in DOA estimation using measured data. The objective was to obtain better angular resolution of the DOA of received signals in angular power spectra by compensating for mutual coupling.

This report is organized as follows. Sections 2 and 3 briefly describe the measurement system and DOA estimation techniques used to collect and analyze the data presented in [1]. Section 4 discusses the theoretical radiation pattern for the four-element array that one expects in the absence of mutual coupling. This is followed in Section 5 by a discussion of mutual coupling effects and the feasibility of compensating for mutual coupling in DOA estimation using either modeling or measured data. Section 6 presents conclusions and recommendations for future DOA measurements, should such measurements be undertaken.

---

[1] The author is with the Institute for Telecommunication Sciences, National Telecommunications and Information Administration, U.S. Department of Commerce, Boulder, CO 80305.

[2] P. Wilson and P. Papazian, private communication.

2. MEASUREMENT SYSTEM

The data in [1] were collected with a digital channel probe (DCP). The DCP generates a maximal-length pseudonoise (PN) code that biphase modulates a radio frequency (RF) carrier. The signal is transmitted over the radio channel, and at the receiver the signal is downcoverted to an intermediate frequency, digitized, and further downconverted to baseband. The baseband signal is cross-correlated with a copy of the transmitted PN code, thereby enabling one to develop the complex, baseband impulse response of the radio transmission channel as a function of time delay. System details are described in a previous report [2]. For these measurements the DCP was configured to transmit a 511-bit PN code at 10 Mb/s using a 1920 MHz RF carrier. The received signal was sampled at 40 Mb/s. Figure 1 shows a calibration impulse and an example of a received impulse; the received impulse shows the effect of multipath.

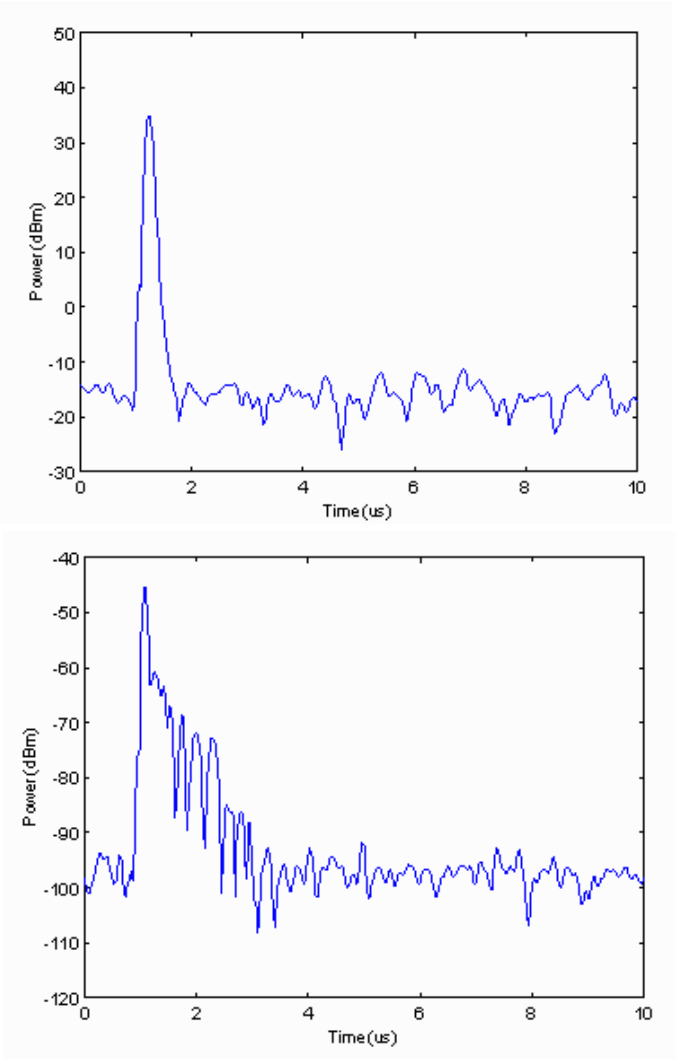

Figure 1. Examples of measured impulses.

A mobile transmitting antenna and a stationary receiving antenna array were used. The transmitting antenna was vertically-oriented and omni-directional with 6.7 dBi gain and a 17.5° vertical 3-dB beamwidth. The antenna was mounted at a height of 2.4 m above ground on a van equipped with a GPS receiver used to tag the data with GPS locations.

The receiving array consisted of four vertically-oriented omni-directional PCS band antennas, each with 8 dBi gain and a 12.0° vertical 3-dB beamwidth. The vertical (E-plane) radiation pattern of each antenna is shown in Figure 2. These four antennas were arranged horizontally in a linear array with half-wavelength spacing. The array was mounted on a rooftop 7 m above ground. RF absorber panels (25 cm cones) were placed directly behind the array so that only the forward-looking 180° sector was considered.

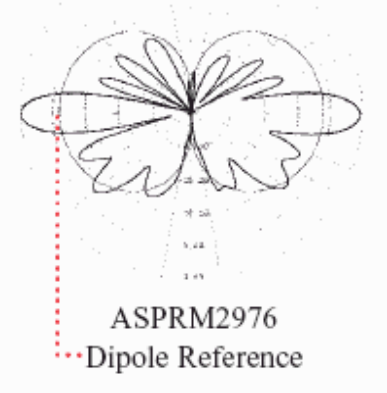

Figure 2. Radiation pattern of the individual antenna elements in the receiving array.

3. DATA ANALYSIS

The DOA estimates discussed in [1] were obtained from azimuth power spectra (APS) that were developed from the impulse response data as follows. A direction-dependent weight vector $\mathbf{w}(\theta)$ is applied to the impulse response vector of the array $\mathbf{x}(\tau)$ to form a scalar $y(\theta,\tau)$:

$$y(\theta,\tau) = \boldsymbol{w}^{H}(\theta)\boldsymbol{x}(\tau) \ , \tag{1}$$

where H denotes the Hermitian conjugate. The estimated power output $P(\theta,\tau)$ is given by

$$P(\theta,\tau) = yy^{*} = \boldsymbol{w}^{H}\boldsymbol{x}\boldsymbol{x}^{H}\boldsymbol{w} = \boldsymbol{w}^{H}(\theta)\boldsymbol{R}_{xx}(\tau)\boldsymbol{w}(\theta) \ , \tag{2}$$

where * denotes the complex conjugate and $\mathbf{R}_{xx}$ defines the autocorrelation matrix. Due to noise and other uncertainties the autocorrelation matrix is not known precisely and was therefore averaged using the modified covariance method (MCM) to obtain a smoothed autocorrelation matrix $\mathbf{R}_{MCM}$ [1].

The weight vectors used weights of equal magnitude with phase differences that correspond to the delay for a plane wave incident from the pointing direction. The weight vector for a four-element, equally spaced, linear array is therefore

$$\boldsymbol{w}(\theta) = (1, e^{-jkd\cos\theta}, e^{-jk2d\cos\theta}, e^{-jk3d\cos\theta})^{T} \ , \tag{3}$$

where θ is the angle of an incident plane wave relative to the array axis, k is the wavenumber, and d is the element spacing. The DOA pattern is obtained by scanning the weight vector over a range of possible angles.

Two DOA estimation methods were considered in [1]: the parallelogram method (PM) and the normalized maximum likelihood method (NMLM). The PM power density is estimated as

$$P_{PM}(\theta,\tau) = \boldsymbol{w}^{H}(\theta)\boldsymbol{R}_{MCM}(\tau)\boldsymbol{w}(\theta) \tag{4}$$

and the NMLM power density estimate is given by

$$P_{NMLM}(\theta,\tau) = \frac{\boldsymbol{w}^{H}(\theta)\boldsymbol{R}_{MCM}^{-1}(\tau)\boldsymbol{w}(\theta)}{\boldsymbol{w}^{H}(\theta)\boldsymbol{R}_{MCM}^{-2}(\tau)\boldsymbol{w}(\theta)} \ . \tag{5}$$

These two power density estimates each define an azimuth delay power spectrum (ADPS) for the measured data. The power delay profile, or delay power spectrum (DPS), and the azimuth power spectrum (APS) are found by performing the appropriate integrations:

$$P(\tau) = \int P(\theta,\tau)d\theta \qquad DPS \tag{6}$$

and

$$P(\theta) = \int P(\theta,\tau)d\tau \qquad APS. \tag{7}$$

The mobile transmitter was driven through a suburban neighborhood, and 223 bursts consisting of 16 impulses each were acquired with a spacing of 5 s between bursts. The 16 impulses in each burst were averaged using MCM and an ADPS was calculated for each burst using both PM and NMLM. Figures 3 (PM) and 4 (NMLM) show an example ADPS, along with the associated APS amd DPS profiles, for the same burst. Both methods show significant multipath.

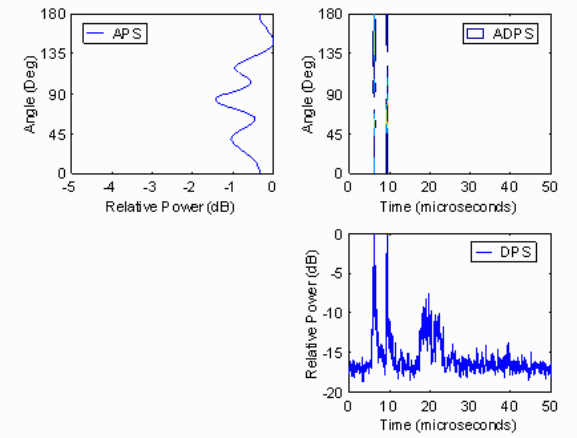

Figure 3. The PM estimated azimuthal delay power spectrum for a sample burst.

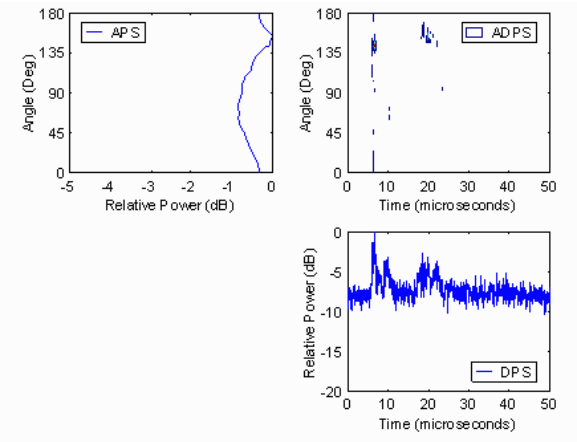

Figure 4. The NMLM estimated azimuthal delay power spectrum for a sample burst.

Figure 5 shows the DOA as determined by three different estimates. The GPS location of the mobile can be used to determine the line-of-sight (LOS) angle. The maxima of the PM and NMLM APS profiles give two further estimates. Whereas the GPS DOA tracks the location of the vehicle, the APS DOA estimates may differ from the LOS value if significant multipath is present. Figure 5 shows a systematic offset of approximately 10° between the GPS LOS value and the two APS estimates. This suggests the presence of systematic errors due to unequal cable lengths or contributions due to the antenna array or other hardware.

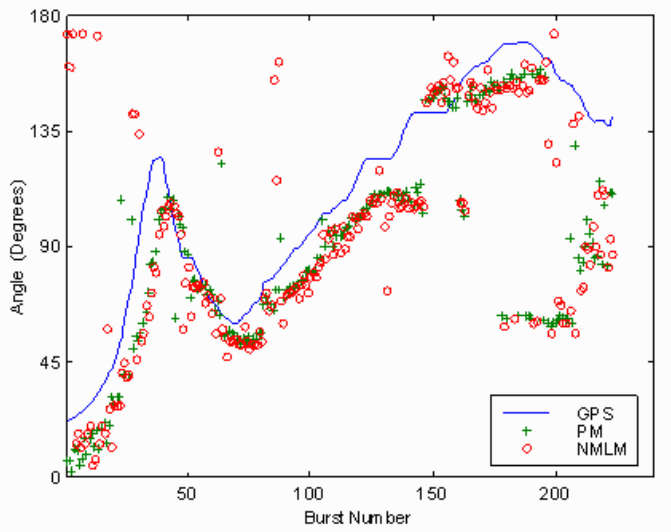

Figure 5. The DOA as determined by the GPS location, the maximum of the PM estimate, and the maximum of the NMLM estimate.

The DPS and APS profiles were used to calculate delay and azimuth spreads. Delay spread was calculated about the mean in the usual way [2] using a 10-dB-below-peak cutoff value. The azimuth spread was calculated about the GPS-determined LOS value using a 3-dB cutoff. The results for the PM and NMLM estimates are shown in Figures 6 and 7, respectively. In particular, note that the angular spreads vary between approximately zero and 90° or more.

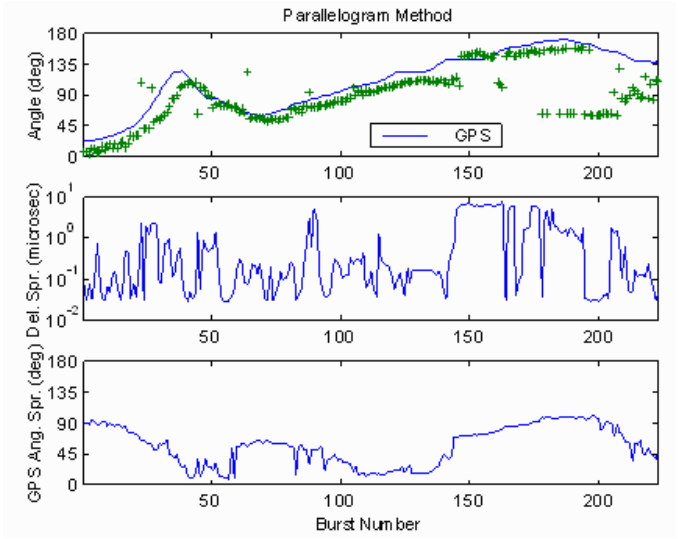

Figure 6. The PM estimates for the DOA, delay spread, and angular spread (about the GPS LOS value).

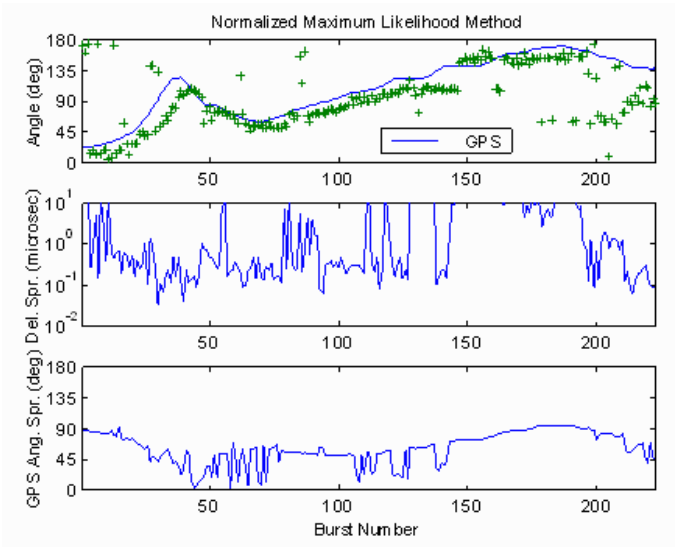

Figure 7. The NMLM estimates for the DOA, delay spread, and angular spread (about the GPS LOS value).

4. RADIATION PATTERN OF A FOUR-ELEMENT ARRAY

Before discussing the effects of mutual coupling on the performance of the antenna array, it is worthwhile to consider the theoretical radiation pattern of the array in the absence of mutual coupling. The normalized radiation pattern $F(\theta,\varphi)$ of an array consisting of identical elements is [3]

$$F(\theta,\varphi) = g(\theta,\varphi)\, f(\theta,\varphi) , \tag{8}$$

where $g(\theta,\varphi)$ is the (normalized) pattern of a single element (the element pattern) and $f(\theta,\varphi)$ is the (normalized) pattern of an array of isotropic point sources with the same locations, amplitudes, and phases as the original array (the array factor).

The array in [1] used vertically-oriented omni-directional antennas arranged horizontally in a linear array. It follows that the radiation pattern in the horizontal plane is simply the array factor in the horizontal plane. For an array of N equally spaced elements with a linear phase progression (the relative phase between adjacent elements is the same), the array factor is [3]

$$f(\psi) = \frac{\sin(N\psi/2)}{N\sin(\psi/2)} , \tag{9}$$

where

$$\psi = kd\cos\theta + \alpha \tag{10}$$

and the $n+1^{th}$ element leads the n^{th} element in phase by α.

With the radiation pattern of the array given by the above expression for $f(\psi)$, it can be shown that the direction θ_0 of the main beam depends on the element separation d and the phase progression α, and that the angular width of the main beam depends on the array length Nd and the main beam pointing angle θ_0. A common measure of the width of the main beam is the half-power beamwidth (HP). Approximate expressions (that become exact in the limit of very long arrays) for HP are [4]

$$HP \approx 0.866\frac{\lambda}{Nd}\csc\theta_0 \qquad near\ broadside \tag{11}$$

and

$$HP \approx 2\sqrt{0.866\frac{\lambda}{Nd}} \qquad endfire. \tag{12}$$

These expressions imply that a four-element array with half-wavelength separation has a half-power beamwidth of approximately 25° near broadside and 76° at endfire. These relatively large beamwidths suggest that the broad APS profiles in Figures 3 and 4 and the 3-dB cutoff angular spreads in Figures 6 and 7 are due to the poor angular resolution of a four-element array and are not due to a failure to compensate for mutual coupling. Moreover, the data contain significant multipath, which may increase the angular spreads to values greater than the theoretical beamwidths.

5. MUTUAL COUPLING

In a real antenna array the elements interact with one another and alter the currents and impedances from what would exist if the elements were isolated. This interaction, called mutual coupling, changes the magnitude, phase, and distribution of current on each element and results in a total array radiation pattern that differs from the theoretical pattern in the no-coupling case.

The impedance effects of mutual coupling can be described by treating an array of N elements as an N-port network using conventional circuit analysis. The current-voltage relations are

$$\begin{aligned} V_1 &= Z_{11} I_1 + Z_{12} I_2 + \cdots + Z_{1N} I_N \\ V_2 &= Z_{21} I_2 + Z_{22} I_2 + \cdots + Z_{2N} I_N \\ &\vdots \\ V_N &= Z_{N1} I_1 + Z_{N2} I_2 + \cdots + Z_{NN} I_N \end{aligned} \tag{13}$$

where V_n and I_n are the impressed voltage and current, respectively, in the n^{th} element and Z_{nn} is the self-impedance of the n^{th} element when all other elements are open-circuited. The mutual impedance Z_{mn} (= Z_{nm} by reciprocity) between the two elements m and n is the open-circuit voltage produced at element m divided by the current supplied to element n when all other elements are open-circuited. Mutual impedance is difficult to compute or measure in general. The technique for measuring mutual impedance between two antennas is discussed in [3] and [4, pp. 157-160], and can be generalized to determine the mutual impedance between any two elements in an arbitrary array.

Closely related to the mutual and self impedances are the S-parameters, which have been measured for the antenna array in [1] using a network analyzer described in [5]. The S-parameters provide a means for characterizing an N-port network inserted in a transmission line. For example, consider the 2-port network (2-element array) inserted in a transmission line shown in Figure 8. The voltage and current along the transmission line can be considered to be in the form of traveling waves. Each of the four traveling waves is made up of a combination of two waves. For example, E_{r2} is made up of that portion of E_{i2} reflected from the output port of the network and that portion of E_{i1} that is transmitted through the network. The S-parameters relate those waves reflected from the network to those waves incident upon the network:

$$\begin{aligned} E_{r1} &= S_{11} E_{i1} + S_{12} E_{i2} \\ E_{r2} &= S_{21} E_{i1} + S_{22} E_{i2} \end{aligned} \tag{14}$$

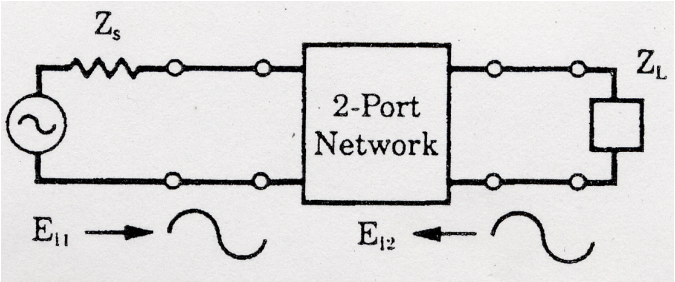

Figure 8. The four traveling waves resulting from the insertion of a two-port network in a transmission line.

On the other hand, the total voltage and total current on the transmission line are given by

$$\begin{aligned} V_1 &= E_{i1} + E_{r1} \\ V_2 &= E_{i2} + E_{r2} \end{aligned} \tag{15}$$

and

$$\begin{aligned} I_1 &= \frac{E_{i1} - E_{r1}}{Z_0} \\ I_2 &= \frac{E_{i2} - E_{r2}}{Z_0} \end{aligned} \tag{16}$$

where Z_0 is the characteristic impedance of the transmission line.

Relationships between the S-parameters S_{ij} and the impedance matrix Z_{ij} can be derived by substituting the expressions for total voltage (15) and total current (16) into the voltage-current relations (13) with N = 2 and rewriting the resulting equations in the form of (14). Equating the coefficients of E_{i1} and E_{i2} in these equations with the corresponding coefficients S_{ij} in (14) implies that

$$S_{11} = \frac{\left(\frac{Z_{11}}{Z_0} - 1\right) - \frac{Z_{12}Z_{21}}{Z_0^2}\left(1 + \frac{Z_{22}}{Z_0}\right)^{-1}}{\left(\frac{Z_{11}}{Z_0} + 1\right) - \frac{Z_{12}Z_{21}}{Z_0^2}\left(1 + \frac{Z_{22}}{Z_0}\right)^{-1}} \tag{17}$$

and

$$S_{12} = \frac{\frac{Z_{12}}{Z_0} - \frac{Z_{12}}{Z_0}\left(1 + \frac{Z_{22}}{Z_0}\right)^{-1}\left(\frac{Z_{22}}{Z_0} - 1\right)}{\left(1 + \frac{Z_{11}}{Z_0}\right) - \frac{Z_{12}Z_{21}}{Z_0^2}\left(1 + \frac{Z_{22}}{Z_0}\right)^{-1}} \tag{18}$$

Expressions for S_{22} and S_{21} can be obtained from these expressions simply by interchanging 1 and 2, since the equations above are invariant under interchange of 1 and 2. Determination of the mutual and self impedances therefore requires solving three relatively complicated coupled equations (assuming reciprocity, so that $Z_{12} = Z_{21}$).

The point is that for an N-element array, one has to solve $N(N + 1)/2$ coupled equations to determine the impedance matrix from measured S-parameters, assuming reciprocity so that Z_{ij} is a symmetric matrix. A four-element array therefore requires solving 10 complicated coupled equations and is therefore not a practical method for determination of the mutual impedances and their effect on the antenna array pattern. Moreover, uncertainties in the measured values of the S-parameters would propagate through the 10 equations, resulting in an impedance matrix of dubious accuracy.

An alternative to measuring mutual impedance is to compute it using numerical methods, such as the method of moments [3, Chapt. 10], [6]. The use of such methods requires a detailed knowledge of the structure of the antenna elements. This is not available for the antenna elements used in [1]. It is clear from the element pattern in Figure 2 that the elements are not simple dipoles, for example. However, they are omnidirectional in azimuth. One can therefore get a rough sense of the effects of mutual coupling on the pattern of the antenna array from examples of patterns of linear arrays of (omnidirectional) dipoles computed with and without mutual coupling.

One such example, taken from [3, Chapt. 10], is shown in Figure 9. The array in this example is a linear array of 12 equally spaced ($d = \lambda/2$), parallel, center-fed, half-wave dipoles phased for a beam maximum 45° off broadside. A 1-volt generator is placed at the center port of each dipole. The normalized patterns are shown for unloaded voltage generator excitations (Figure 9(a)) and for 72-Ω loaded voltage generator excitations (Figure 9(b)). The solid curves are the patterns for an array with ideal current generators (no mutual coupling), and the dashed curves are the patterns for an array with voltage generators (mutual coupling present), computed using the method of moments. Thus, the differences between the solid and dashed curves are due to the effects of mutual coupling. There is little difference in the three normalized patterns and no apparent difference in the main beamwidths in Figure 9, suggesting that the effects of mutual coupling on the array in [1] may also be small.

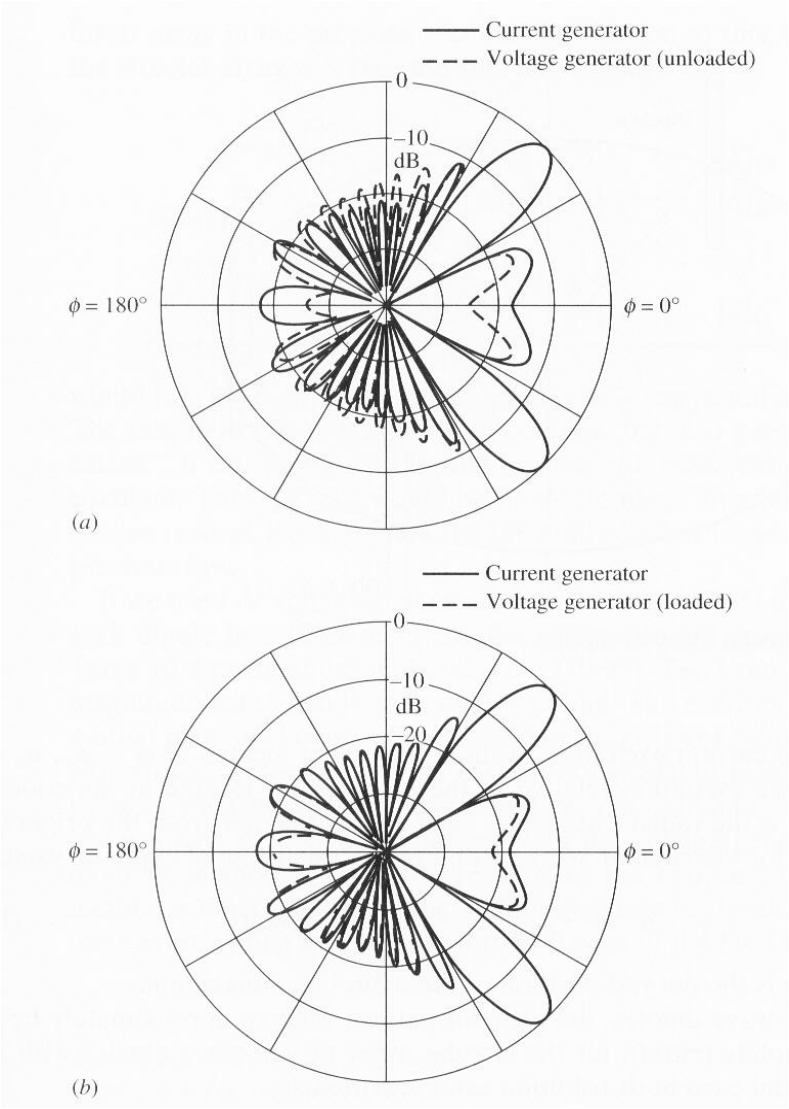

Figure 9. Linear array patterns for 12 equally spaced half-wave dipoles with main beam steered to 45° off broadside and ideal current generators (solid curve) compared to patterns from an array with voltage generators. (a) Linear array pattern for unloaded voltage generator excitations (dashed curve). (b) Linear array pattern for 72-Ω loaded voltage generator excitations (dashed curve). (Figure 10-27, p. 467, in W.L. Stuzman & G.A. Thiele, *Antenna Theory and Design*, New York: John Wiley & Sons, Inc., ©1998. Reprinted with permission of John Wiley & Sons, Inc.)

The effects of mutual coupling on array patterns are smaller for larger arrays. In the limit of infinitely large arrays, each element in an array of equally spaced identical elements sees the same operating environment. Thus, the impedances of all the elements are equal, and the normalized pattern is unchanged by mutual coupling [3], [6]. In smaller arrays, edge effects become more significant and the effects of mutual coupling on array pattern are more pronounced. The effects of mutual coupling on the array in [1] may therefore be larger than those in Figure 9, but its effects are still expected to be small, particularly on the width of the main beam.

6. CONCLUSIONS AND RECOMMENDATIONS

The relatively poor angular resolution of the four-element array discussed in [1] is consistent with the theoretical radiation pattern of such an array in the absence of mutual coupling. The effects of mutual coupling on the array performance would be difficult to measure or to model, but in any case are not expected to be significant. Furthermore, the bias between the GPS-determined DOA and the DOA as determined from the APS profiles implies the presence of a systematic error that could not be eliminated by compensating for mutual coupling. Finally, it should be recognized that the measured data reported in [1] contain significant multipath and that the APS profiles developed from Equation (7) include this multipath because the integral over time delay was not cut off after the time of the direct arrival.

Based on these conclusions the following recommendations are suggested if such measurements are undertaken in the future. Before making field measurements, the antenna array should be calibrated in a simple RF environment that is well-understood, e.g., an antenna test range or an anechoic chamber. The measured amplitude and phase responses of the individual elements would then enable one to use a corrected weight vector $w(\theta)$ in the data analysis that would compensate for systematic errors as well as any mutual coupling effects that are present. On the other hand, attempting to compensate for mutual coupling effects by measurements or modeling of mutual impedances would be neither feasible nor necessary. Finally, before comparing measured APS profiles to the expected array pattern, the integral over time delay in Equation (7) should be cut off after the direct arrival time (100 ns for the measurement system in [1]), thereby eliminating multipath effects.

7. REFERENCES

[1] P. Wilson and P. Papazian, "PCS band direction-of-arrival measurements using a 4-element linear array," in *Proc. of the IEEE Vehicular Technology Conference*, Boston, MA, Sep. 24-28, 2000.

[2] P. Wilson, P. Papazian, M. Cotton, and Y. Lo, "Advanced antenna test bed characterization for wideband wireless communication systems," NTIA Report 99-369, Aug. 1999.

[3] W. L. Stutzman and G. A. Thiele, *Antenna Theory and Design*, Ch. 3, New York: John Wiley & Sons, Inc., 1998.

[4] R. C. Hansen, Ed., *Microwave Scanning Antennas*, Vol. II, *Array Theory and Practice*, New York: Academic Press, 1966, pp. 23-29.

[5] Agilent AN 154 S-Parameter Design Application Note, Agilent Technologies.

[6] C. A. Balanis, *Antenna Theory: Analysis and Design*, Ch. 8, New York: John Wiley & Sons, Inc., 1997.